Nuclear Physics B165 (1980) 80–92

EVENT SHAPES IN DEEP INELASTIC LEPTON-HADRON SCATTERING*

Geoffrey C. FOX, Tsun-Yan TSE and Stephen WOLFRAM**
California Institute of Technology, Pasadena, California 91125

Received 22 August 1979

The structure of hadronic final states in deep inelastic scattering expected from QCD is analyzed in terms of the shape parameters H_l and C_l. We find that the effects of the fragmentation of quarks and gluons into hadrons are typically governed by $\sqrt{s} = [Q^2(1/x-1)]^{\frac{1}{2}}$. For $\sqrt{s} \gtrsim 30$ GeV, the distributions of events in H_2 and C_2 should allow a test of the perturbative QCD prediction of three-jet events.

1. Introduction

According to the original parton model, the hadron final state of a deep inelastic lepton–hadron scattering event should consist of two jets: one initiated by the struck quark and the other arising from the fragments of the target nucleon from which the quark was ejected. In QCD, three-jet events should also occur, in which, for example, the outgoing quark radiates a gluon with high transverse momentum, thereby forming a third jet of hadrons. The investigation of such processes provides a probe of QCD perturbation theory beyond the leading logarithmic approximation so far used in analysis of the total deep inelastic cross section. In this paper, we describe a method for analyzing the structure of hadron final states in deep inelastic scattering, which should (at least at energies $\sqrt{s} \simeq \sqrt{Q^2(1/x-1)} \gtrsim 30$ GeV) allow a precise test of the QCD prediction for three-jet final states to be made. To characterize the distributions of hadronic energy or 'shapes' of events we use the observables H_l, originally introduced for the analysis of e^+e^- annihilation final states [1], together with the C_l, which are two-dimensional analogues of the H_l, as discussed in [1, 2]. For small l, these observables probe only the gross structure of the final state, and are not sensitive to details of the hadrons in the final state, which were presumably formed at times of order $1/\Lambda$ where perturbative methods are irrelevant. The formal consequence of this insensitivity is that the $\langle H_l \rangle$ and $\langle C_l \rangle$ are infrared stable when computed in QCD perturbation theory, so that divergences

* Work supported in part by the U.S. Department of Energy under Contract No. DE-AC-03-79ER0068.
** Feyman Fellow.

which appear in their calculation may be controlled. These points, with some mention of deep inelastic scattering, are discussed at length in [1, 2].

We define

$$H_l \equiv \sum_{i,j} \frac{|p_i||p_j|}{s} P_l(\hat{p}_i \cdot \hat{p}_j) \equiv \left(\frac{4\pi}{2l+1}\right) \sum_{m=-l}^{+l} \left| \sum_i Y_l(\Omega_i) \frac{|p_i|}{\sqrt{s}} \right|^2 , \tag{1.1}$$

where the sums on i and j run over all particles in the final state (except, of course, the scattered lepton), and $\sqrt{s}$ is the total energy available for the formation of hadrons, given in deep inelastic scattering, by

$$s \simeq Q^2 \left(\frac{1}{x} - 1\right), \tag{1.2a}$$

where, as usual, the Bjorken variable x is defined as

$$x = \frac{Q^2}{2m_N \nu}. \tag{1.2b}$$

Q is the invariant mass and ν the energy of the intermediate virtual photon or W/Z (usually referred to simply as γ^*). The values of the H_l for an event depend on the frame in which the particle momenta are evaluated; we shall throughout consider only the γ^*-nucleon center of mass frame. Any other choice of frame must ultimately yield the same physical results. From the definition (1.1) one sees that (for massless final particles) energy conservation implies $H_0 = 1$, when the sum is performed over the complete final state. Experimentally, some particles will presumably go undetected: this may roughly be compensated by dividing all the H_l found using the observed particles by H_0 [1]. (An analogous procedure may be used for the C_l defined below.)

The H_l describe the distribution of energy on a hypothetical sphere surrounding a deep inelastic scattering event. The fact that they do not single out any direction in space is very convenient for the analysis of e^+e^- annihilation events where no natural axis is defined in the final state. However, in deep inelastic scattering, the momentum of the exchanged γ^* (or W*) provides a natural direction, and one may consider the distribution of hadron energy around this direction, as characterized by

$$C_l = \sum_{i,j} \frac{(p_\perp)_i (p_\perp)_j}{s} \cos\left[l(\phi_i - \phi_j)\right] \equiv \left| \sum_i \frac{(p_\perp)_i}{\sqrt{s}} e^{il\phi_i} \right|^2 , \tag{1.3}$$

where the particle i has azimuthal angle ϕ_i and magnitude of momentum $(p_\perp)_i$ projected on the plane perpendicular to the γ^* direction. C_0 therefore gives simply the square of the total transverse momentum of the final hadrons with respect to the γ^* direction. The higher-order C_l provide a complete description of the transverse momentum distribution. Note that $C_1 = 0$ by momentum conservation, but C_{2l+1}, $l > 0$ need not vanish.

Further details on the structure of events in deep inelastic scattering are afforded by consideration of the angular distribution of hadronic energy with respect to the incoming lepton direction. This is parametrized by the observables [1]

$$D_l \equiv \sum_i \frac{(p_\perp)_i}{\sqrt{s}} \cos\left(l(\phi_b - \phi_i)\right), \tag{1.4}$$

where ϕ_b is the azimuthal angle defined by the projection of the incoming lepton direction onto the plane orthogonal to the γ^*.

For spin-1 exchanges between the lepton and hadron systems, $\langle D_l \rangle = 0$ for $l > 2$, and in all cases $D_0 = C_0$. The D_l provide an infrared stable formulation of the tests of QCD originally suggested in [3]. In terms of the D_l (and making the choice $\phi_b = 0$)

$$\begin{aligned}
&\sum_i (p_\perp)_i/\sqrt{s} = D_0 = C_0\,,\\
&\sum_i ((p_\perp)_i/\sqrt{s}) \cos\phi_i = D_1 = 0\,,\\
&\sum_i ((p_\perp)_i/\sqrt{s}) \cos(2\phi_i) = D_2\,,\\
&\sum_i ((p_\perp)_i/\sqrt{s}) |\cos\phi_i| = \frac{2}{\pi}(D_0 + 2D_2/3)\,,
\end{aligned} \tag{1.5}$$

where in the last case, we have suppressed the infinite series of higher-order D_l which must vanish when averaged over events. In e^+e^- annihilation, the B_l observables which are analogous to the D_l for that case were of rather limited value, mainly because they suffered particularly severely from hadron fragmentation effects. We suspect that the D_l will be beset by similar difficulties, and we shall not discuss them further here.

2. Results

For an idealized two-jet event, it is clear that, as in e^+e^- annihilation,

$$H_{2l} = 1\,, \qquad H_{2l+1} = 0\,. \tag{2.1}$$

Three-jet final states introduce $0(\alpha_s)$ modifications to these results, and the formation of hadrons from the quarks and gluons typically gives $0(\Lambda/\sqrt{s})$ corrections. Note that transverse momentum ("Fermi motion") of the initial quark with respect to the incoming nucleon direction has very little effect on the $\langle H_l \rangle$, because of their rotational invariance. It merely makes a slight boost on the final state momenta.

An idealized two-jet event has no transverse momentum with respect to the γ^* direction, and therefore gives

$$C_l = 0 . \tag{2.2}$$

A three-particle or ideal three-jet final state gives*

$$C_{2l} = C_{2l'} = 4(p_\perp{}^2)_{\text{jet}}/s , \qquad C_{2l+1} = 0 . \tag{2.3}$$

Fragmentation leads to deviations from these results, as would four-jet final states (at $O(\alpha_s^2)$). An event in which the hadronic energy is distributed in an azimuthally-symmetrical manner about the incoming proton (and hence target fragment) direction will give

$$C_0 = \left[\frac{\sum_i (|p_\perp|)_i}{\sqrt{s}}\right]^2 , \qquad C_l = 0 , \qquad (l > 0) . \tag{2.4}$$

This is approximately the case for two-jet hadronic events, except for a small offset resulting from transverse momentum of the initial quark with respect to the nucleon direction. In our phenomenological estimates, we include a Gaussian distribution of initial quark transverse momentum (and the corresponding momentum for the target fragments) with a generous $\langle k_\perp \rangle = 600$ MeV, but its effects are in all cases entirely negligible. The emission of a gluon from the quark struck by the γ^* or W* should not affect the fragments of the target nucleon from which the quark was ejected. Their contribution to the C_l for three-jet events is therefore roughly the same as for two-jet events. The fragmentation of the quark and gluon produced in $\gamma^* q \to qG$ into hadrons spreads out their energies and tends to diminish the $\langle C_{2l} \rangle$.

A possible complication in the analysis of deep inelastic event shapes arises from the possibility of high transverse momentum photon emissions from incoming or outgoing legs. One effect of these is to deflect the incoming or scattered lepton, and therefore to alter the direction of the virtual photon inferred from their measurement. This spread in momentum of the photon gives similar effects to the Fermi motion of the incoming quark, and its consequences are probably likewise negligible, even for the C_l. Photon emissions from the final state modify the shapes of events in the same manner as do gluon emissions, but the smallness of $\alpha_{\text{e.m.}}$ compared to α_s makes them irrelevant for our estimates.

In appendix B we give the differential cross sections for the three-jet production processes $\gamma^* q \to qG$ and $\gamma^* G \to q\bar{q}$, whose kinematics are discussed in appendix A. In estimating these cross sections, we assume (without profound theoretical justification) that the relevant effective coupling is $\alpha_s(Q^2) \simeq 1.5/\log (Q^2/(0.5\ \text{GeV})^2)$. The precise forms of the cross sections depend on the preparation of the virtual photon, and hence on the component of the scattered lepton angular

* For this result, we take the fragments of the target to lie along the γ^* direction, and the two produced partons to have equal and opposite transverse momenta $(p_\perp)_{\text{jet}}$.

distribution or structure fraction sampled. Appendix B gives results for the various cases (including the parity-violating F_3 component accessible from νN-$\bar{\nu}$N); the shapes of the final states are entirely insensitive to which is considered*. (For the calculation presented below, we assumed that the direction of the final lepton was uniformly averaged over, selecting the $g_{\mu\nu}$ projection of $W_{\mu\nu}$.) For the longitudinal momentum distributions of the incoming partons, we used the fits obtained in ref. [4] for a proton target. Different choices for these distributions (which give the x dependence of the total γ^*N cross section) cancel out in considering the final state shapes except at large x, where they can make factor of two changes. It turns out that events from the process $\gamma^*G \to q\bar{q}$ tend to be closer to two-jet by a factor typically $\gtrsim 10$ than those from $\gamma^*q \to qG$, so that the dominant three-jet processes in QCD should be of the latter type. In eq. (B.4) we give the differential cross-section for the process $\gamma^*q \to q\phi$, where ϕ is a scalar 'gluon'. This process gives rise to events whose shapes are comparable to those from $\gamma^*G \to q\bar{q}$ in QCD. The observation of large three-jet effects would therefore discriminate against scalar gluon theories and support QCD.

The most important uncertainty in the calculation of the shapes of hadronic events is the fragmentation of the quarks and gluon produced at short distances, into the observed hadrons. The purpose of considering infrared stable shape parameters is to control the incalculable large distance effects, but at forseeable energies, their consequences will still be felt, and one must adopt a phenomenological model to estimate them. We use the model developed by Field and Feynman [5], which provides a satisfactory fit to present data on two-jet final states. In the formation of hadrons, a third jet will not be resolved unless it has a sufficiently high transverse momentum. We use the prescription that in events arising from subprocesses for which $H_2 > 0.8$, hadrons are produced in two jets, while if $H_2 < 0.8$, the fragmentation of the third jet is treated independently. The implementation of this method and its sensitivity to the precise value of the H_2 cut was discussed at length in [1]; use of the more precise methods suggested in [2] should not affect our rough phenomenological estimates. In addition to considering the formation of hadrons from the struck quark (and any high energy gluons emitted by it), we must also treat hadron production from the fragments of the nucleon target, since, in our shape parameter analysis, all particles in the final state are included. We assume that the target fragments just like a quark, which should be reasonable at least for the dominant $\gamma^*q \to qG$ process**. The target fragments should also radiate gluons,

* The contribution from longitudinal photons is typically less than 0.1%. The projection $g_{\mu\nu}W^{\mu\nu}$ selects the cross-section combination $\sigma_T - \sigma_L/2 \simeq \sigma_T$.

** This form is reasonable for low momentum fragments since the rapidity plateau associated with the fragmentation of the "diquark" left after a quark in the proton has been ejected by the γ^*, should be similar to that for a quark. In addition, at high momenta, the $q \to \pi$ fragmentation model of ref. [5] should also roughly describe diquark fragmentation, except that in the latter case, the leading particle is an N rather than a π. However, the type of the final hadrons is not important for our analysis.

but since the momenta transferred to them from the struck quark will typically not be large, the radiation will not be very important, and cannot lead to three-jet events. One may consider cuts on the final state designed to remove the contribution of target fragments. We gave some discussion of such phenomenological devices in [1], and will not elaborate here.

Fig. 1 shows the distributions of events expected in the shape parameters H_2, C_0, C_2 and C_4, at $Q^2 = 100\,\mathrm{GeV}^2$ and $x = 0.1$. The essential parameter in deter-

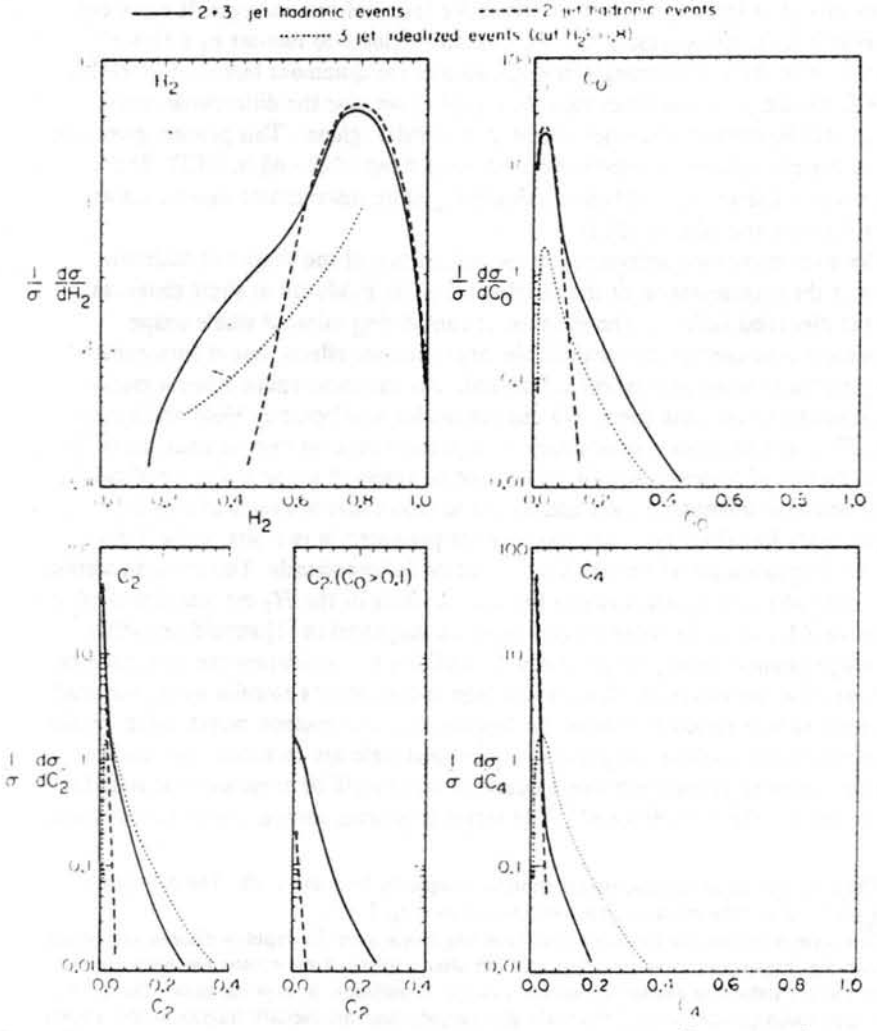

Fig. 1. Distributions of shape parameters in deep inelastic scattering for $Q^2 = 100\,\mathrm{GeV}^2$ and $x = 0.1$.

mining the modifications due to fragmentation is $\sqrt{s} = (Q^2(1/x - 1))^{\frac{1}{2}} \approx 30$ GeV in this case. The H_2 distributions in fig. 1 are roughly similar to the analogous ones for e^+e^- annihilation events at the same value of $\sqrt{s}$ discussed in [1]. The three-jet events at this $\sqrt{s}$ give rise to a significant tail in the H_2 distribution, which is evident in fig. 1. Although distinctive, this tail corresponds to only 6% of all hadronic events having $H_2 < 0.5$; 1.4% of the quark–gluon systems from which they came had $H_2 < 0.5$. It is clear from fig. 1 that the low H_2 tail of three-jet events is much modified by fragmentation. Thus the observation of a tail is even at $\sqrt{s} =$ 30 GeV only a qualitative and not a quantitative test of QCD. Notice that in e^+e^- annihilation, three-jet effects are much larger; 9% of idealized three-jet events have $H_2 < 0.5$, and after fragmentation the fraction is roughly doubled. Nevertheless, it is clearly worthwhile to study QCD effects in many different ways. In our curves for hadronic final states, we have included all particles in the calculation of the H_l and C_l. Ref. [1] showed, however, that better agreement between results for idealized and hadronic events could be achieved by using only particles with momentum greater than some cut, which was conveniently taken at 0.5 GeV. This device can also be used for deep inelastic scattering events.

The broadening in the C_0 distributions for hadronic events results from the transverse momenta of the hadrons from the struck quark and target fragments, as given by eq. (2.4). The target fragments, and, for two-jet events, the struck quark products should be distributed roughly symmetrically in azimuth around the incoming γ^* direction. Such systems give little contribution to the C_l for $l > 0$ (see eq. (2.4)), and hence the C_2 and C_4 distributions for two-jet events are much narrower than the corresponding C_0 distributions. The C_2 and C_4 distributions for three-jet events receive little contribution from target fragmentation, so that hadron fragmentation serves only to soften the distributions, as for the H_{2l}. As expected, the effect is more pronounced for C_4 than for C_2, since C_4 probes the events at smaller angular scales than C_2, so that hadronic effects are more important. At $\sqrt{s} =$ 30 GeV shown in fig. 1, both $(1/\sigma)\,\mathrm{d}\sigma/\mathrm{d}C_0$ and $(1/\sigma)\mathrm{d}\sigma/\mathrm{d}C_2$ exhibit significant tails due to three-jet effects. For C_0, 6% of events lie in the tail above $C_0 = 0.12$, while for C_2, there is a 2% tail at $C_2 > 0.06$; in each case there is negligible two-jet contamination above this cut. A still better separation of three-jet events is afforded by considering the C_2 distributions of events for which the total transverse momenta of the final particles satisfy a cut, which for the curve given in fig. 1 was taken as $C_0 > 0.1$. (This cut includes 9% of all events.) The cut $C_0 > 0.1$ removes many of the two-jet final states; the C_2 distribution of the remaining events therefore provides a test for the dynamical mechanism of three-jet production. Azimuthally-symmetric fragmentation of a two-particle event (which violates $C_0 = 0$ by virtue of fragmentation transverse momentum) leads to much smaller values of C_2 than the three-jet final states expected in QCD. Before fragmentation, QCD predicts $\langle C_2/C_0 \rangle \equiv 1$ for three-jet events; unfortunately, however, this is much modified by fragmentation, and $\langle C_2/C_0 \rangle = 0.13$ (0.24) for $C_0 < 0.1$ ($C_0 > 0.1$) with hadronic events in the kinematic regime of fig. 1. Some features of the shapes of

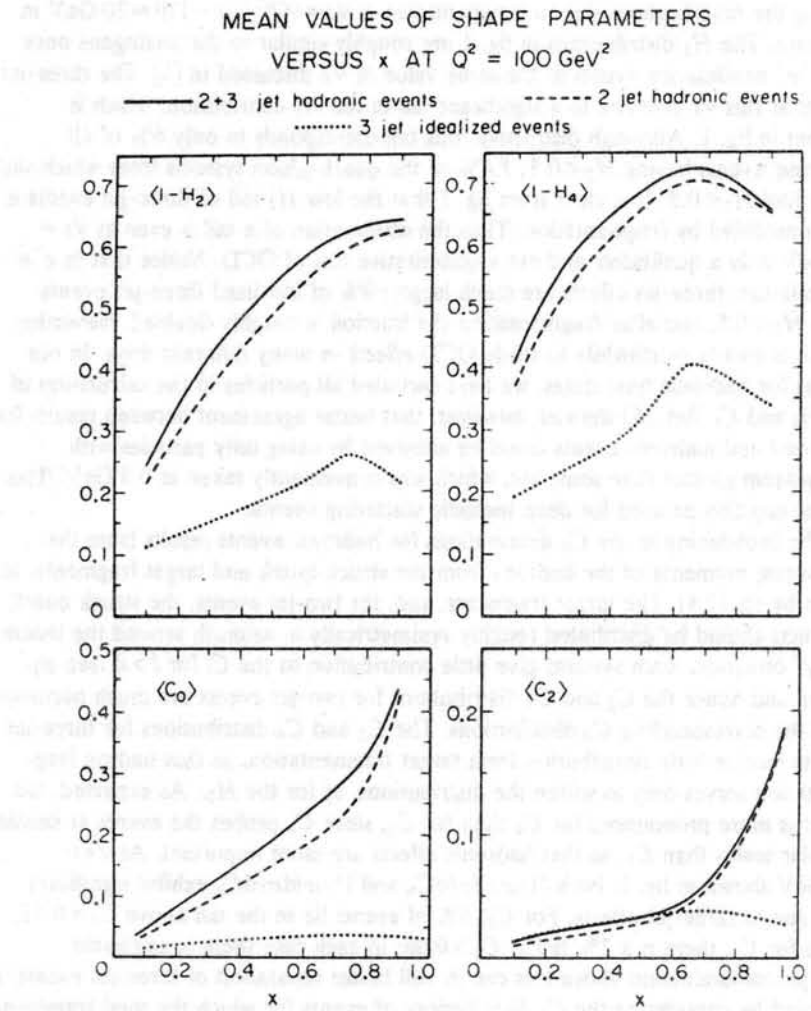

Fig. 2. Mean values of shape parameters in deep inelastic scattering as a function of x for $Q^2 = 100\ \mathrm{GeV}^2$.

events may be summarized by giving the mean values of shape parameters for them. Of course, in doing this one loses the effects of the distinctive three-jet tails (as they only correspond to a small fraction of the events) in the distributions of events in the shape parameters. This is very evident in fig. 2 where the mean shape parameters are plotted as a function of the Bjorken variable x. In [1], we noted that in the free quark and gluon approximation, three-jet effects in the mean shape

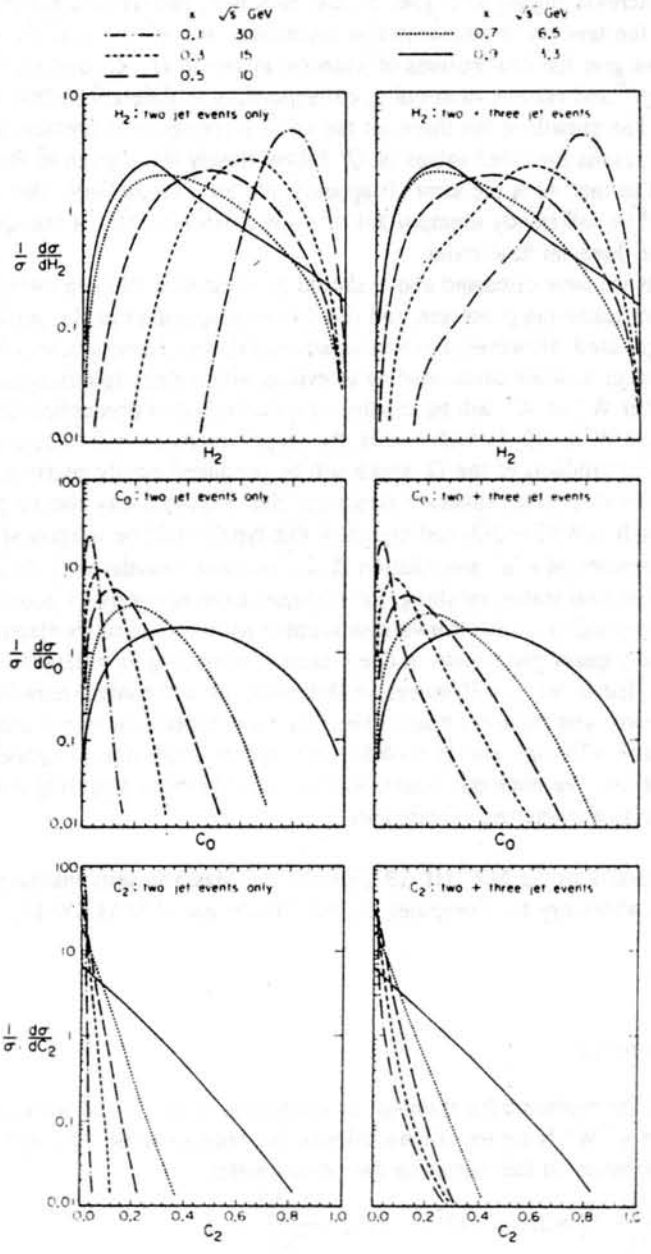

Fig. 3. The x (or $\sqrt{s}$ dependence) of the distribution of shape parameters for deep inelastic scattering events at $Q^2 = 100\ \mathrm{GeV}^2$.

parameters increase slightly as x goes to one. However, this trend is entirely overwhelmed by the severity of fragmentation corrections as $x \to 1$ (so that $\sqrt{s} \to 0$).

In fig. 3 we give the distributions of hadronic events in H_2, C_0 and C_2 for $Q^2 = 100\ \mathrm{GeV}^2$ and various values of x, corresponding to different hadron system energies $\sqrt{s}$. The growth of the three-jet tail as $\sqrt{s}$ increases (x decreases) is very evident. The results for other values of Q^2 follow closely those given in fig. 3, once x is adjusted so that $\sqrt{s}$ is the same. It appears that for $\sqrt{s} \gtrsim 30$ GeV, hadronic effects should be sufficiently unimportant to allow a definitive test of the QCD prediction for three-jet final states.

The effects we have discussed above should be present in all deep inelastic lepton–hadron scattering processes, and should be independent of the particular beam or target used. However, the production and decay of heavy flavors of quarks should also occur in some cases, leading to events with a more spherical shape. Typically either W^+ or W^- will be capable of inducing direct production of heavy quarks through $W^{\pm}q \to Q$. In such events, the target fragments will form one jet, while the decay products of the Q, which will be produced mostly nearly at rest, should give rise to a rather spherical structure. Heavy quarks may also be produced in pairs through $\gamma(W)G \to Q\bar{Q}$, and events of this type should be roughly spherical.

In our discussion of e^+e^- annihilation [1, 2], we have considered in detail the several possible final states, resulting, for example, from heavy quark production and decay. It would be straightforward to supplement our qualitative statements above on heavy quark production in deep inelastic scattering by a detailed analysis analogous to that in ref. [1]. However, in this paper we will content ourselves with the study of two- and three-jet final states. Our basic conclusion is that useful tests of QCD require γ^*N c.m. energy $\sqrt{s} \gtrsim 30$ GeV; rather larger than is necessary in e^+e^- annihilation. We hope our results will be useful to those analyzing and planning deep inelastic scattering experiments.

We are grateful to the MATHLAB group of the Massachusetts Institute of Technology Laboratory for Computer Science for the use of MACSYMA.

Appendix A

Three-jet kinematics

We define the momenta for three-jet production as in fig. 4, and work, as always, in the $\gamma^*(W^*)$N center of mass system. We take $\sqrt{s}$ to be the c.m.s. energy in the γ^*N collision, so that (ignoring the proton mass)

$$s = Q^2\left(\frac{1}{x} - 1\right) = 2m_N\nu - Q^2, \qquad E_N = \frac{s + Q^2}{2\sqrt{s}},$$
$$x = \frac{Q^2}{2m_N\nu}, \qquad E_2 = E_{\gamma^*} = \frac{s - Q^2}{2\sqrt{s}}. \tag{A.1}$$

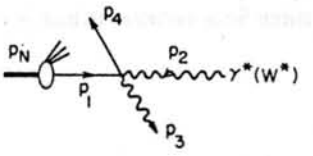

Fig. 4. The kinematics of three-jet production in γ^*N collisions. 1 is the initial parton; 2 the initial γ^* while 3 and 4 are the final state partons. The final state "diquark" (fragments of the nucleon) is not labeled in the figure.

For the $2\to 2$ subprocess, we define the kinematic invariants

$$\begin{aligned}
&\hat{s}=(p_1+p_2)^2=Q^2\left(\frac{\xi}{x}-1\right), && \hat{s}+\hat{t}+\hat{u}=-Q^2,\\
&\hat{t}=(p_1-p_3)^2=2E_1E_3(\cos\eta_3-1), && -(\hat{s}+Q^2)\leqslant\hat{t}\leqslant 0,\\
&\hat{u}=(p_1-p_4)^2=2E_1E_4(\cos\eta_4-1), &&
\end{aligned} \tag{A.2}$$

and we take the angle between $\boldsymbol{p}_3(\boldsymbol{p}_4)$ and the γ^* direction ($\boldsymbol{p}_2$) to be $\eta_3(\eta_4)$. $\xi(\geqslant x)$ is the fraction of the nucleon's momentum (p_N) carried by the incoming parton (p_1). We assume here that p_1 has no component transverse to p_N. Then one finds

$$E_3=\frac{[(\hat{t}-Q^2)\xi-\hat{t}]x+Q^2\xi^2}{2\xi\sqrt{Q^2x(1-x)}}, \qquad \cos\eta_3=\frac{x[\hat{t}(2x-1)+\xi(Q^2-\hat{t})]-Q^2\xi^2}{\xi x(Q^2-\hat{t})+\hat{t}x-Q^2\xi^2}. \tag{A.3}$$

E_4 and $\cos\eta_4$ are obtained by replacing $\hat{t}$ in eq. (A.3) with $\hat{u}$. In the limit $\xi\to 1$, (A.3) reduces to

$$E_3=\tfrac{1}{2}\sqrt{s}=E_4, \qquad \cos\eta_3=\cos\eta_4=\frac{2\hat{t}+s+Q^2}{s+Q^2}=\frac{2\hat{t}x+Q^2}{Q^2}. \tag{A.4}$$

The energy of the remnants of the nucleon ('diquark') after the ejection of momentum p_1 is

$$E_d=(1-\xi)E_N=\frac{Q^2(1-\xi)}{2\sqrt{Q^2x(1-x)}}. \tag{A.5}$$

The fractional energies of the three final particles (which are all taken to be massless) are therefore:

$$x_1 = \frac{2E_d}{\sqrt{s}} = \frac{(1-\xi)}{(1-x)},$$

$$x_2 = \frac{2E_3}{\sqrt{s}} = \frac{[(\hat{t}-Q^2)\xi - \hat{t}]x + Q^2\xi^2}{Q^2\xi(1-x)},$$

$$x_3 = \frac{2E_4}{\sqrt{s}} = \frac{[(\hat{t}+Q^2)\xi - \hat{t}]x - Q^2\xi}{Q^2\xi(x-1)}. \tag{A.6}$$

In terms of these, one finds, for example,

$$H_2 = 1 - \frac{6(1-x_1)(1-x_2)(1-x_3)}{x_1x_2x_3}$$

$$= 1 + \frac{6\hat{t}(1-\xi)x(x-\xi)(\hat{t}x+Q^2\xi)}{[\xi x(\hat{t}-Q^2)+Q^2\xi^2-\hat{t}x][\xi x(\hat{t}+Q^2)-Q^2\xi-\hat{t}x]}. \tag{A.7}$$

For $\xi \to 0$, this becomes $H_2 \simeq 1$, and for $\xi \to 1$,

$$H_2 \simeq 1 + \frac{6\hat{t}x(Q^2+\hat{t}x)}{Q^4}\frac{(1-\xi)}{(1-x)}. \tag{A.8}$$

Appendix B

Three-jet cross sections

For the diagrams of fig. 5, one finds, using the kinematics defined in appendix A:

$$g_{\mu\nu}W^{\mu\nu} = -2\left(\frac{4g^2}{3}\right)\left[\frac{\hat{s}}{\hat{t}}+\frac{\hat{t}}{\hat{s}}-\frac{2Q^2\hat{u}}{\hat{s}\hat{t}}\right], \qquad (p_1)_\mu(p_1)_\nu W^{\mu\nu} = (\tfrac{4}{3}g^2)\hat{u}, \tag{B.1}$$

where $W^{\mu\nu}$ is the 'hadron tensor,' and the factors in parentheses are from color averaging. For the diagrams in fig. 6, one obtains (by crossing):

$$g_{\mu\nu}W^{\mu\nu} = 2\left(\frac{g^2}{2}\right)\left[\frac{\hat{u}}{\hat{t}}+\frac{\hat{t}}{\hat{u}}-\frac{2Q^2\hat{s}}{\hat{u}\hat{t}}\right], \qquad (p_1)_\mu(p_1)_\nu W^{\mu\nu} = (\tfrac{1}{2}g^2)(-\hat{s}). \tag{B.2}$$

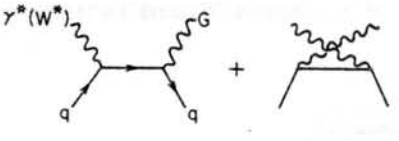

Fig. 5. Feynman diagrams for $\gamma^*q \to qG$.

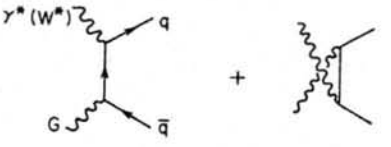

Fig. 6. Feynman diagrams for $\gamma^*G \to q\bar{q}$.

If one takes the W*-quark coupling to be $\gamma_\mu(1+\lambda\gamma_5)$, then all the results in eqs. (B.1) and (B.2) are multiplied by $(1+\lambda^2)$, and for the process of fig. 5

$$i\epsilon_{\mu\nu\alpha\beta}(p_3)^\alpha(p_1)^\beta W^{\mu\nu}$$
$$= \lambda\left(\frac{4g^2}{3}\right)\left[-\frac{4Q^6}{\hat{s}\hat{t}} - 4Q^4\left[\frac{1}{\hat{s}}+\frac{2}{\hat{t}}\right] - 2Q^2\left[\frac{3\hat{s}}{\hat{t}}+\frac{\hat{t}}{\hat{s}}\right] - 2\frac{\hat{s}^2}{\hat{t}} + 2\hat{t}\right]. \tag{B.3}$$

For colored scalar gluons, eq. (B.1) becomes

$$g_{\mu\nu}W^{\mu\nu} = -\left(\frac{4g^2}{3}\right)\frac{(\hat{s}+\hat{t})^2}{\hat{s}\hat{t}}. \tag{B.4}$$

References

[1] G.C. Fox and S. Wolfram, Phys. Rev. Lett. 41 (1978) 1581; Nucl. Phys. B149 (1979) 413.
[2] G.C. Fox and S. Wolfram, A gallimaufry of e^+e^- annihilation event shapes, Caltech preprint CALT 68-723 (1979).
[3] H. Georgi and H.D. Politzer, Phys. Rev. Lett. 40 (1978) 3;
A. Mendez and T. Weiler, QCD predictions for jet transverse momentum in lepto-production, Oxford preprint 93/78 (1978).
[4] G.C. Fox, Nucl. Phys. B131 (1977) 107.
[5] R.D. Field and R.P. Feynman, Nucl. Phys. B136 (1978) 1.